

## Evidence for Radial-Energy Scaling of Nonequilibrium Neutron Yield in Damped $^{139}\text{La} + ^{40}\text{Ar}$ Reactions

J. L. Wile,<sup>(a)</sup> S. S. Datta,<sup>(b)</sup> R. T. de Souza,<sup>(c)</sup> J. R. Huizenga, D. Pade,<sup>(d)</sup> W. U. Schröder, and J. Töke

*Departments of Chemistry and Physics and Nuclear Structure Research Laboratory,  
University of Rochester, Rochester, New York 14627*

(Received 14 August 1989)

Emission patterns of neutrons from damped  $^{139}\text{La} + ^{40}\text{Ar}$  reactions at  $E_{\text{lab}} = 400$  and  $600$  MeV, mostly consistent with sequential evaporation from accelerated fragments, reveal the existence of a high-energy component at all kinetic energy losses. The average multiplicity associated with this nonequilibrium component is found to scale with the radial kinetic energy at contact, with a threshold of  $E_{\text{rad}} \approx 2$  MeV/nucleon. Boltzmann-master-equation and Fermi-jet models disagree with the data, the latter model requiring enhanced high-momentum components.

PACS numbers: 25.70.Lm

Since the early days of heavy-ion nuclear physics, observation of emission patterns of light particles has constituted one of the basic and widely acknowledged tools of probing a large variety of aspects of heavy-ion-induced reactions.<sup>1</sup> At low bombarding energies, a few MeV per nucleon above the Coulomb barrier, such patterns were found to reflect the relatively gentle character of the collisions, with most of the light-particle yield explainable in terms of a "late" emission from thermally equilibrated reaction products. At these low energies, therefore, the observed light-particle yield can be cast into the form of an incoherent sum of contributions associated with respective moving sources, the heavy reaction products. In particular, a single moving source—the compound nucleus—was found adequate in the case of fusion reactions leading to evaporation residues, while two sources—two thermally equilibrated reaction fragments—proved necessary in the case of either damped or fusion-fission-like reactions. At higher bombarding energies, the complexity of light-particle emission patterns increases, reflecting shorter emission times and the onset of more violent, dynamical emission mechanisms. At these higher energies, inspection of Galilei-invariant two-dimensional velocity-vector distributions of light particles,  $v_{\perp}$  vs  $v_{\parallel}$ , reveals the presence of components whose centers of gravity coincide with neither of the above-mentioned equilibrated emission sources. These components are associated with fast, nonequilibrium emission mechanisms.<sup>2,3</sup>

In order to shed more light on the onset of these nonequilibrium emission mechanisms in damped collisions, the  $^{139}\text{La} + ^{40}\text{Ar}$  reaction was studied at two laboratory energies of 400 and 600 MeV.<sup>4,5</sup> Damped reactions are especially well suited to study nonequilibrium emission phenomena. Through the total kinetic energy loss, they provide a simple experimental measure of the impact parameter, a quantity that influences strongly the probability of nonequilibrium particle emission.

The experiments, carried out at the 88-in. cyclotron facility of the Lawrence Berkeley Laboratory, consisted of measurements of neutron energy spectra at different

laboratory angles in coincidence with heavy reaction fragments. In these experiments, a  $^{40}\text{Ar}$  beam bombarded a  $500\text{-}\mu\text{g}/\text{cm}^2$  self-supporting  $^{139}\text{La}$  target placed in the center of a thin-walled scattering chamber. Neutron energy spectra were measured simultaneously at seven angles using a time-of-flight (TOF) technique. The start signal for the TOF measurements was provided by a heavy-fragment telescope placed near the grazing angle, detecting predominantly projectilelike fragments (PLF) from damped collisions. This PLF telescope provided, at the same time, an identification of the reaction channel according to total kinetic energy loss  $E_{\text{loss}}$  and the (secondary) fragment atomic number  $Z$ . The respective stop signals for the TOF were provided by seven NE213 scintillator detectors placed at different angles and at distances approximately 1 m from the target. Pulse-shape discrimination was employed to suppress the  $\gamma$ -ray background. Details of the experimental setup and of the analysis scheme are described elsewhere.<sup>4,5</sup>

Inspection of the exclusive neutron yields in the Galilei-invariant representation of  $v_{\perp}$  vs  $v_{\parallel}$  revealed the presence of a component, distinct from the two dominant ones associated with the fully accelerated and equilibrated projectilelike and targetlike fragments. The average velocity vector of this additional component is aligned with the beam axis and has a magnitude of approximately one-half of the beam velocity, independent of both  $E_{\text{loss}}$  and  $Z$  of the PLF. Such characteristics are commonly interpreted as signatures of emission during the early stages of the collision, a phenomenon often termed "preequilibrium" emission. Numerically, the total experimental neutron yield was decomposed into three components using a seven-parameter fitting procedure. The individual contributions were assumed to show a Maxwellian energy dependence and an isotropic angular distribution in their respective reference frames. The validity of such simple assumptions was ultimately checked by the quality of the final fits to the data. The seven adjustable parameters included spectral slopes and multiplicities of the neutrons of the three sources, and the (effective) velocity of the nonequilibrium emitter.

In Fig. 1, systematics of the average multiplicity ( $\langle m_{\text{pre}} \rangle$ ) of the nonequilibrium component are shown as a function of total kinetic energy loss,  $E_{\text{loss}}$ . Data obtained at  $E_{\text{lab}}=400$  MeV are indicated by triangles, whereas the circles represent data at 600 MeV. Error bars reflect statistical errors, errors of background subtraction, and uncertainties of the yield decomposition procedure. At both bombarding energies, a distinct linear correlation is observed between  $\langle m_{\text{pre}} \rangle$  and  $E_{\text{loss}}$ . However, these correlations show different strengths at the two bombarding energies, demonstrated by the different slopes for the two lines fitted to the respective sets of data points. Hence, the energy loss does not constitute a universal scaling parameter for  $\langle m_{\text{pre}} \rangle$  at different bombarding energies, suggesting that the correlations seen in Fig. 1 result from a more fundamental dependence of both  $E_{\text{loss}}$  and  $\langle m_{\text{pre}} \rangle$  on common dynamical collision parameters.

The search for a possible dynamical scaling law for nonequilibrium emission led to Fig. 2. In this figure, the nonequilibrium neutron multiplicity is plotted versus radial energy per nucleon at contact,  $E_{\text{rad}}(R_{\text{SA}})/\mu$ . The contact distance is assumed, for sake of simplicity, to be equal to the strong absorption radius  $R_{\text{SA}}$ . Conversion from the representation of Fig. 1 to that of Fig. 2 requires knowledge of the correlation between the radial energy at contact and  $E_{\text{loss}}$ . According to the stochastic

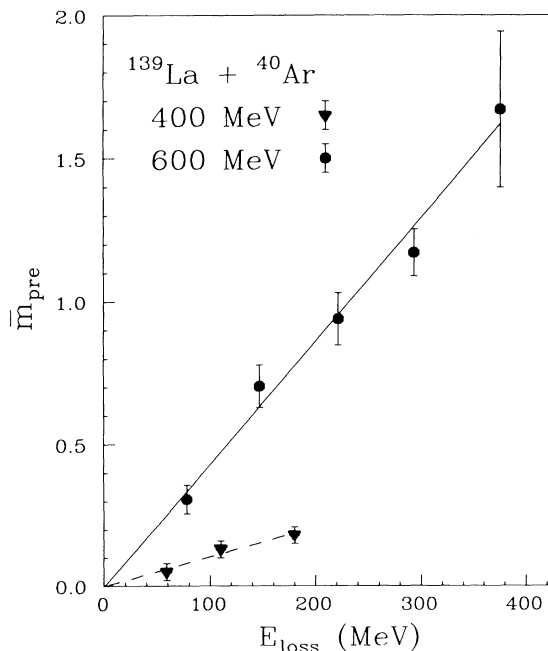


FIG. 1. Correlations between the multiplicity of nonequilibrium neutrons and the total kinetic energy loss at  $E_{\text{lab}}=400$  (triangles) and 600 MeV (circles). The lines are linear fits to the respective set of data points. Error bars reflect statistical errors, errors of background subtraction, and uncertainties of the yield decomposition procedure.

nucleon-exchange model,<sup>6,7</sup> this correlation depends on the bombarding energy. Quantitatively, the classical trajectory code CLAT (Ref. 8) based on the one-body transport model<sup>6,7</sup> was employed to predict the correlation between  $E_{\text{loss}}$  and the relative angular momentum and, hence, between  $E_{\text{loss}}$  and the radial energy at contact. Since the code CLAT is unable to handle cases of extreme kinetic energy losses, approaching the limit of full energy relaxation, associated with large fragment deformations, Fig. 2 contains fewer data points on the  $^{139}\text{La} + ^{40}\text{Ar}$  reaction than does Fig. 1. As seen in Fig. 2, the experimental points for both bombarding energies define one common curve. This observation suggests that the radial energy at contact is a proper scaling parameter for the nonequilibrium emission process, at least for a fixed projectile-target system. At the same time, such a scaling is compatible with the view that nonequilibrium emission occurs during the early collision stages. Additionally, the dependence seen in Fig. 2 suggests that the nonequilibrium emission mechanism has a threshold. The mechanism sets in rapidly at  $E_{\text{rad}}(R_{\text{SA}})/\mu \approx 2$  MeV/nucleon. It is tempting to speculate that, in the particular representation of Fig. 2, the position of the threshold might be independent of the projectile-target combination involved. On the other hand, the rate at which the probability of nonequilibrium emission grows with increasing  $E_{\text{rad}}(R_{\text{SA}})/\mu$  could well scale additionally with, e.g., the sizes of the nuclei involved, or with the total number of neutrons in the system. Validity of the above speculations based on the  $^{139}\text{La} + ^{40}\text{Ar}$  reactions at two energies is supported by the set of data points shown in Fig. 2 as squares. These additional data points are based on recently published data on preequilibrium neutron emission from the damped  $^{165}\text{Ho} + ^{58}\text{Ni}$  reaction at 930 MeV.<sup>9</sup> The latter points indicate that, indeed, within

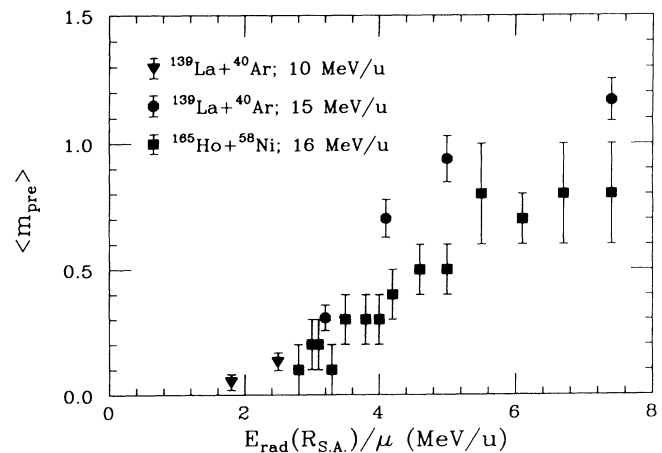


FIG. 2. Average multiplicity of nonequilibrium neutrons from the reaction  $^{139}\text{La} + ^{40}\text{Ar}$  at  $E_{\text{lab}}=400$  (triangles) and 600 MeV (circles) and from the reaction  $^{165}\text{Ho} + ^{58}\text{Ni}$  at 930 MeV (Ref. 9) (squares), as a function of the radial kinetic energy at contact.

the uncertainties of the experimental and analysis procedures, the threshold for preequilibrium emission of neutrons for this heavier system is the same as it is for the lighter  $^{139}\text{La} + ^{40}\text{Ar}$  system studied in this paper. The relevant data on the conversion from  $E_{\text{loss}}$  to  $E_{\text{rad}}(R_{\text{SA}})$  for the three sets of data points shown in Fig. 2 is summarized in Table I.

The experimental data were compared with two types of theoretical models. In the first set of model calculations, the Fermi-jet code of Randrup and Vandenbosch<sup>10</sup> was employed. The existence of the Fermi-jet mechanism, originally proposed by Bondorf,<sup>11</sup> is a natural and important implication of the one-body transport mechanism.<sup>6,7</sup> In recent years, a model based on this latter mechanism has enjoyed considerable success in describing quantitatively various aspects of damped reactions.<sup>1</sup> It has also provided an intuitive and qualitative framework for understanding many other aspects of heavy-ion reactions. Results of the Fermi-jet-model calculations for the  $^{139}\text{La} + ^{40}\text{Ar}$  reaction at 600 MeV are shown in Fig. 3 by dotted and thin solid lines. The dotted lines represent the Fermi-jet spectra obtained with the original model. The dashed lines are the summed spectra including Fermi-jet and evaporation contributions associated with PLF and TLF. These dashed lines clearly fail to account for the experimental multiplicities of high-energy neutrons. In order to improve the fit to the experimental data, it is necessary to enhance the high-momentum components of the Fermi distribution as compared with the Fermi-gas-model prediction. In the Fermi-jet calculations illustrated in Fig. 3 by thin solid curves, such an enhancement was simulated by increasing the Fermi-gas temperature by a factor of 2. The resulting summed spectra are shown in Fig. 3 as thick solid lines. The enhancement of the high-momentum component of the Fermi distribution, required to obtain the fit, is somewhat incompatible with the one-body transport model and with the Fermi-jet model. It does not

TABLE I. Angular momentum dependence of  $E_{\text{loss}}$  predicted by the stochastic nucleon-exchange model code CLAT,<sup>8</sup> and used in the evaluation of  $E_{\text{rad}}(R_{\text{SA}})$ .

Reaction	$E_{\text{lab}}$ (MeV)	$E_{\text{loss}}$ (MeV)	$l$
$^{139}\text{La} + ^{40}\text{Ar}$	400	60	178
		110	162
	600	80	240
		145	226
		225	210
$^{165}\text{Ho} + ^{58}\text{Ni}$	930	295	165
		112	363
		212	347
		312	323
		412	268

come, however, as a complete surprise. Similar enhancement of the high-momentum components of the Fermi distribution was earlier reported necessary to explain, e.g., features observed in the energy spectra of neutrons accompanying fusion reactions<sup>12</sup> and muon capture in complex nuclei.<sup>13,14</sup> Theoretically, such enhancements are thought to arise from nucleon-nucleon correlations, i.e., two-body effects beyond the scope of the one-body transport model.

As an alternative, a model based on the Boltzmann master equation was used in the form developed by Blann.<sup>15</sup> As can be seen in Fig. 4, this approach experiences difficulties in explaining the observed neutron spectra. No satisfactory fit to the experimental data could be obtained, even with a large variation in the value of the crucial model parameter  $n_0$ , that represents the initial number of excitons present in the system.

In summary, a nonequilibrium component has been identified in the emission patterns of neutrons accompanying the damped reactions  $^{139}\text{La} + ^{40}\text{Ar}$  at  $E_{\text{lab}} = 400$  and 600 MeV. The average multiplicity of neutrons associated with this component shows a distinct linear

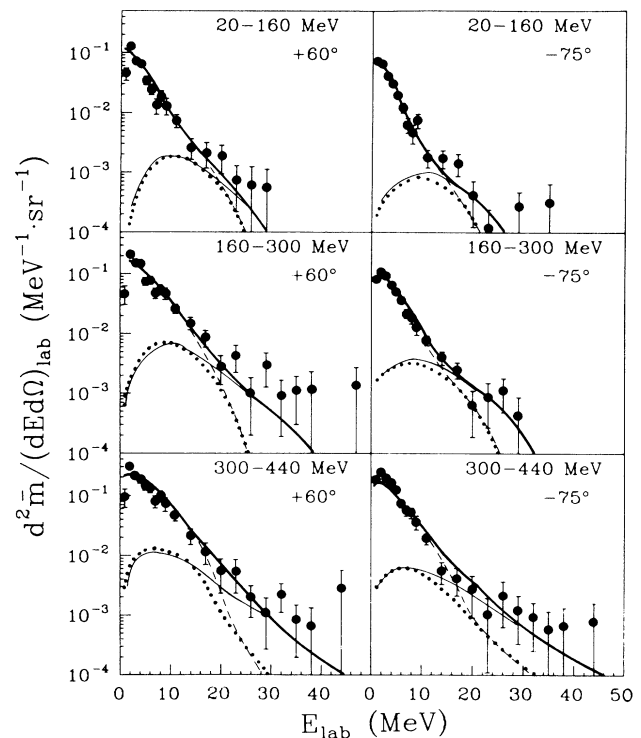


FIG. 3. Results of the Fermi-jet-model calculations at  $E_{\text{lab}} = 600$  MeV obtained with default values for the basic model parameters (dotted line) and enhanced high-momentum components (thin solid line). The summed spectra, including Fermi-jet and the evaporation contributions associated with PLF and TLF, are shown as dashed and thick solid lines, respectively. Experimental spectra are represented by dots with error bars.

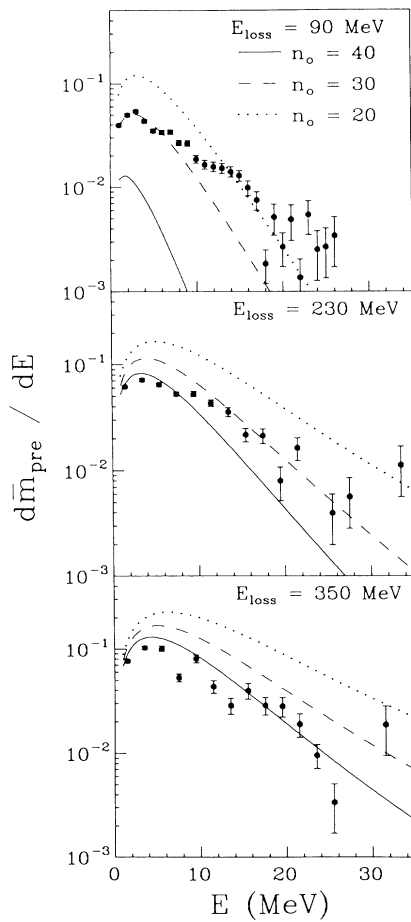


FIG. 4. Comparison of the experimental integrated non-equilibrium neutron spectra for different energy-loss bins with results of the Boltzmann-master-equation model. Three different values of the initial number of excitons in the system,  $n_0=20$  (dotted line),  $n_0=30$  (dashed line), and  $n_0=40$  (solid line) are probed.

correlation with  $E_{\text{loss}}$ , dependent on bombarding energy, implying a scaling with the radial kinetic energy at contact. In such a scaling, the nonequilibrium emission mechanism has a threshold at  $E_{\text{rad}}(R_{\text{SA}})/\mu \approx 2$  MeV/nucleon. No satisfactory description of the experimental high-energy neutron spectra was obtained within the framework of either the Fermi-jet or the Boltzmann-master-equation models. A fit to the experimental neutron spectra was, however, obtained, using the Fermi-jet

model with enhanced high-momentum components of the Fermi distribution.

This work was supported by the U.S. Department of Energy under Grant No. DE-FG02-88ER40414.

<sup>(a)</sup>Present address: Indiana University, Bloomington, IN 47405.

<sup>(b)</sup>Present address: Panjab University, Chandigarh 160014, India.

<sup>(c)</sup>Present address: Michigan State University, East Lansing, MI 48824.

<sup>(d)</sup>Present address: Ruhr Universität, 4630 Bochum, West Germany.

<sup>1</sup>W. U. Schröder and J. R. Huizenga, in *Treatise on Heavy-Ion Science*, edited by D. A. Bromley (Plenum, New York and London, 1984), Vol. 2, and references therein.

<sup>2</sup>A. Gavron, J. R. Beene, B. Cheynis, R. L. Ferguson, F. E. Obenshain, F. Plasil, G. R. Young, G. A. Pettitt, C. F. Maguire, D. G. Sarantites, M. Jääskeläinen, and K. Geoffroy-Young, *Phys. Rev. C* **27**, 450 (1983).

<sup>3</sup>D. Hilscher, H. Rossner, A. Gamp, U. Jahnke, B. Cheynis, B. Chambon, D. Drain, C. Pastor, A. Giorni, C. Morand, A. Dauchy, P. Stassi, and G. Pettitt, *Phys. Rev. C* **36**, 208 (1987).

<sup>4</sup>J. L. Wile, S. S. Datta, W. U. Schröder, J. R. Huizenga, J. Töke, and R. T. de Souza, *Phys. Rev. C* **39**, 1845 (1989).

<sup>5</sup>J. L. Wile, S. S. Datta, W. U. Schröder, J. R. Huizenga, R. T. de Souza, and D. Padre, *Phys. Rev. C* **40**, 1700 (1989).

<sup>6</sup>J. Randrup, *Nucl. Phys. A* **307**, 319 (1978); **A327**, 490 (1979); **A383**, 468 (1982).

<sup>7</sup>J. Dössing and J. Randrup, *Nucl. Phys. A* **433**, 215 (1985); **A433**, 280 (1985).

<sup>8</sup>W. U. Schröder, R. T. de Souza, J. R. Huizenga, and L. M. Schmieder, in *Proceedings of the International Symposium on Nuclear Fission in Heavy-Ion Reactions* [Nucl. Sci. Conf. Series **11**, 255 (1987)].

<sup>9</sup>G. A. Pettitt, C. Butler, V. Penumetcha, T. C. Awes, J. R. Beene, R. L. Ferguson, F. E. Obenshain, F. Plasil, G. R. Young, and S. P. Sorensen, *Phys. Rev. C* **40**, 692 (1989).

<sup>10</sup>J. Randrup and R. Vandenbosch, *Nucl. Phys. A* **474**, 219 (1987).

<sup>11</sup>J. P. Bondorf, *J. Phys. C* **5**, 195 (1976).

<sup>12</sup>E. Holub, D. Hilscher, G. Ingold, U. Jahnke, H. Orf, H. Rossner, W. P. Zank, W. U. Schröder, H. Gemmeke, K. Keller, L. Lassen, and W. Lücking, *Phys. Rev. C* **33**, 143 (1986).

<sup>13</sup>M. Lifshitz and P. Singer, *Phys. Rev. C* **22**, 2135 (1980).

<sup>14</sup>W. U. Schröder, U. Jahnke, K. H. Lindenberger, G. Röscher, R. Engfer, and H. K. Walter, *Z. Phys.* **268**, 57 (1974).

<sup>15</sup>M. Bann, *Phys. Rev. C* **23**, 205 (1981); **31**, 1245 (1985).